An Optimization Based Discontinuous Galerkin Approach for High-Order Accurate Shock Tracking

Matthew J. Zahr* and Per-Olof Persson†

Lawrence Berkeley National Laboratory,
University of California, Berkeley,
Berkeley, CA 94720-3840, U.S.A.

This work presents a high-order accurate, nonlinearly stable numerical framework for solving steady conservation laws with discontinuous solution features such as shock waves. The method falls into the category of a *shock tracking* or r-adaptive method and is based on the observation that numerical discretizations such as finite volume or discontinuous Galerkin methods that support discontinuities along element faces can perfectly represent discontinuities and provide appropriate stabilization through approximate Riemann solvers. The difficulty lies in aligning element faces with the unknown discontinuity. The proposed method recasts a discretized conservation law as a PDE-constrained optimization problem whose solution is a (curved) mesh that tracks the discontinuity and the solution of the discrete conservation law on this mesh. The discrete state vector and nodal positions of the high-order mesh are taken as optimization variables. The objective function is a discontinuity indicator that monotonically approaches a minimum as element faces approach the shock surface in a neighborhood of radius $\mathcal{O}(h)$, where h is the mesh size parameter. The discretized conservation law on a parametrized domain defines the equality constraints for the optimization problem. A full space optimization solver is used to simultaneously converge the state vector and mesh to their optimal values. This ensures the solution of the discrete PDE is never required on meshes that are not aligned with discontinuities and it increases the nonlinear stability. The method is demonstrated in one and two dimensions: transonic flow through a nozzle and supersonic flow around a bluff body. In both cases, the framework tracks the discontinuity closely with curved mesh elements and provides accurate solutions on extremely coarse meshes, e.g., $\mathcal{O}(10^3)$ degrees of freedom to resolve supersonic flow at Mach 4 in two dimensions.

I. Introduction

While it is clear that the discontinuous Galerkin (DG) and related high-order methods[1–3] are getting sufficiently mature to handle realistic problems in aerodynamics, they are still suffering from the lack of nonlinear stability. This limits their impact on many important applications, in particular ones involving shocks since even small oscillations in the solution can cause non-physical results.

Several approaches have been proposed for handling shocks. One simple method is to use a sensor that identifies the elements in the shock region and reduce the order of interpolating polynomials.[4,5] This is usually combined with h-adaptivity to better resolve the shocks, and it can be quite satisfactory for in particular steady-state problems. More sophisticated approaches include limiting, for example based on weighted essentially non-oscillatory (WENO) concepts.[1,6] Another popular approach is the artificial viscosity technique for subcell shock capturing presented in Ref. 7 and 8. Inspired by the early artificial viscosity methods,[9] this approach has proven to be surprisingly effective in the context of high-order DG methods. The method combines a highly selective spectral sensor with a consistently discretized artificial viscosity

*Postdoctoral Fellow, Department of Mathematics, Lawrence Berkeley National Laboratory, University of California, Berkeley, Berkeley, CA 94720. E-mail: mjzahr@lbl.gov.

†Associate Professor, Department of Mathematics, University of California, Berkeley, Berkeley CA 94720-3840. E-mail: persson@berkeley.edu.

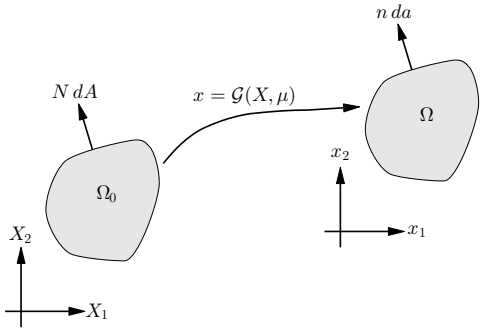

Figure 1: Mapping between reference and physical domains.

added to the equations. This smoothing of the discontinuities gives a number of important benefits, such as fully converged steady-state solutions and smooth behavior of moving shocks.

However, shock capturing techniques such as limiting and artificial viscosity all have the drawback that the accuracy is reduced to first order in the affected elements, which leads to a formal first order global accuracy. While this can be partially offset with appropriate h-adaptivity, in particular using anisotropic elements around the shock, it does pose a major limitation and makes it unclear if high-order methods can be competitive for these applications.

In this work, we present an overview of our high-order DG method for shocks, originally introduced in [10], which is more closely related to shock tracking and r-refinement than shock capturing. It is based on the observations that if a (curved) face of an element is perfectly aligned with a shock, the approximate Riemann solver will provide the appropriate stabilization and allow for high-order approximations of the solution on both sides of the discontinuity. The difficulty with these methods is that the DG method without additional stabilization is highly sensitive to the location of the elements, and a very small mismatch will in general result in oscillations and prevent convergence.

Here, we instead recast the nonlinear, discrete equations as a PDE-constrained optimization problem where the objective function is an appropriate shock indicator, the constraints are the DG discretization of the conservation law, and the optimization variables are the discrete PDE solution and the positions of the nodes of the mesh. The mesh deformation is handled by transforming the conservation law to a fixed reference domain through a diffeomorphism. This means the mesh nodes will be aligned in a consistent way with the current numerical solution (and not, e.g., the true physical position), but also that we can obtain converged solutions using efficient constrained optimization methods. We will present all the components of our framework, and demonstrate high-order convergence of a number of relevant shock problems in 1D and 2D.

II. Governing equations and spatial discretization

Consider a general system of N_c steady, inviscid conservation laws, defined on the physical domain $\Omega \subset \mathbb{R}^d$,

$$\nabla \cdot \mathcal{F}(U) = 0 \quad \text{in } \Omega, \tag{1}$$

where $U(x) \in \mathbb{R}^{N_c}$ is the solution of the system of conservation laws at $x \in \Omega \subset \mathbb{R}^d$ and $\mathcal{F}(U) \in \mathbb{R}^{N_c \times d}$ is the physical flux. We assume that the solution U contains discontinuities, such as shock waves, in which case the conservation law (1) holds away from these discontinuities.

II.A. Transformed conservation law on fixed reference domain

As the goal in this work is to track discontinuities through the deformation of the computational mesh, and therefore the physical domain, it is convenient to reformulate the conservation law on a fixed reference domain, Ω_0. Let $\mathcal{G} : \mathbb{R}^d \times \mathbb{R}^{N_\mu} \to \mathbb{R}^d$ be a parametrized diffeomorphism defining the map from reference to physical domain (Figure 1), i.e.,

$$\Omega = \mathcal{G}(\Omega_0, \mu), \tag{2}$$

where $\mu \in \mathbb{R}^{N_\mu}$ is a vector of parameters. Under the domain mapping (2), the conservation law becomes

$$\nabla \cdot \mathcal{F}(U) = 0 \quad \text{in} \quad \mathcal{G}(\Omega_0,\, \mu). \tag{3}$$

The conservation law on the physical domain Ω is transformed to a conservation law on the reference domain Ω_0 using the procedure in [11] to yield

$$\nabla_X \cdot F(u,\, \mu) = 0 \quad \text{in} \quad \Omega_0 \tag{4}$$

where ∇_X denotes spatial derivatives with respect to the reference domain Ω_0 with coordinates X. The transformed state vector, u, and flux, F, take the form

$$u = g_\mu U, \qquad F(u,\, \mu) = g_\mu \mathcal{F}(g_\mu^{-1} u) G_\mu^{-T} \tag{5}$$

where $G_\mu(X) = \frac{\partial}{\partial X}\mathcal{G}(X,\, \mu)$ is the deformation gradient of the domain mapping and $g_\mu(X) = \det G_\mu(X)$ is the Jacobian. For details regarding the derivation of the transformed equations, the reader is referred to [11].

II.B. Discontinuous Galerkin discretization of transformed conservation law

A standard nodal discontinuous Galerkin method is used to discretize the conservation law (1). Let $\mathcal{E}_{h,p}$ represent a discretization of the domain Ω_0 into non-overlapping, potentially curved, computational elements, where h is a mesh element size parameter and p is the polynomial order associated with the curved elements. The element-wise weak form of the governing equation in (4) results from multiplication by a test function ψ, integration over a single element $K \in \mathcal{E}_{h,p}$, and application of the divergence theorem

$$\int_K \nabla_X \cdot F(u,\, \mu) \cdot \psi \, dV = \int_{\partial K} \psi \cdot F(u,\, \mu) N \, dA - \int_K F(u,\, \mu) : \nabla_X \psi \, dV = 0, \tag{6}$$

where N is the outward normal to the surface ∂K. The global weak form, upon which DG methods are built, arises from the summation of the local residuals over all elements in $\mathcal{E}_{h,p}$

$$\sum_{K \in \mathcal{E}_{h,p}} \int_{\partial K} \psi \cdot F(u,\, \mu) N \, dA - \int_{\Omega_0} F(u,\, \mu) : \nabla_X \psi \, dV = 0. \tag{7}$$

The numerical flux, F^*, is introduced in the first term of (7)

$$\sum_{K \in \mathcal{E}_{h,p}} \int_{\partial K} \psi \cdot F^*(u,\, \mu,\, N) \, dA - \int_{\Omega_0} F(u,\, \mu) : \nabla_X \psi \, dV = 0 \tag{8}$$

to ensure the flux is single-valued along ∂K where u is multi-valued. In the discontinuity-tracking setting, the inter-element jumps will not tend to zero under refinement, which means the numerical flux must be consistent with the governing equation at discontinuities. In this work, Roe's method[12] with the Harten-Hyman entropy fix[13] is used for the numerical fluxes at interior faces and the appropriate boundary conditions determines the numerical fluxes on faces that intersect $\partial\Omega$.

To establish the finite-dimensional form of (8), we introduce the isoparametric finite element space of piecewise polynomial functions associated with the mesh $\mathcal{E}_{h,p}$:

$$\mathcal{V}_{h,p} = \left\{ v \in [L^2(\Omega_0)]^{N_c} \mid v|_K \circ \mathcal{T}_K \in [\mathcal{P}(K_0)]^{N_c} \; \forall K \in \mathcal{E}_{h,p} \right\}$$

where $\mathcal{P}_p(K_0)$ is the space of polynomial functions of degree at most $p \geq 1$ on the parent element K_0 and $K = \mathcal{T}_K(K_0)$ defines a mapping from the parent element to element $K \in \mathcal{E}_{h,p}$. For notational brevity, we assume all elements map from a single parent element. Then the Galerkin weak form in (8) becomes: find $u_{h,p} \in \mathcal{V}_{h,p}$ such that for all $\psi_{h,p} \in \mathcal{V}_{h,p}$

$$\sum_{K \in \mathcal{E}_{h,p}} \int_{\partial K} \psi_{h,p} \cdot F^*(u_{h,p},\, \mu,\, N) \, dA - \int_{\Omega_0} F(u_{h,p},\, \mu) : \nabla_X \psi_{h,p} \, dV = 0. \tag{9}$$

To obtain the discrete form of (9), we introduce a basis $\{\varphi_i\}_{i=1}^{N_p}$ for $\mathcal{P}_p(K_0)$. While this can be any valid basis, a flexibility afford by the DG framework, it is convenient for the proposed shock tracking method to work with a *nodal basis*. Define a set of nodes $\{\xi_j\}_{j=1}^{N_p}$ within the parent element K_0 and let φ_i be the Lagrange polynomial associated with nodes ξ_i over element K_0 with the property $\varphi_i(\xi_j) = \delta_{ij}$. For brevity, we introduce notation for the Lagrange basis defined on the reference element $K \in \mathcal{E}_{h,p}$: $\varphi_i^K(X) = \varphi_i(\mathcal{T}_K^{-1}(X))$. The finite-dimensional solution, $u_{h,p}$, in each element $K \in \mathcal{E}_{h,p}$ is written in terms of its discrete expansion coefficients as

$$u_{h,p}(X)|_K = \sum_{i=1}^{N_p} \boldsymbol{u}_i^K \varphi_i^K(X), \tag{10}$$

where $\boldsymbol{u}_i^K \in \mathbb{R}^{N_c}$ is the solution at node i of element K. Under the isoparametric assumption, the physical coordinates are expanded in the nodal basis as

$$x_{h,p}(X)|_K = \sum_{i=1}^{N_p} \boldsymbol{x}_i^K \varphi_i^K(X), \tag{11}$$

where $\boldsymbol{x}_i^K \in \mathbb{R}^d$ is the coordinate of node i of element K. From this expansion, the deformation gradient, G, and Jacobian, g, required to define the transformed state vector and fluxes are

$$\begin{aligned} G_{h,p}(X)|_K &= \sum_{i=1}^{N_p} \boldsymbol{x}_i^K \frac{\partial \varphi_i^K}{\partial X}(X) \\ g_{h,p}(X)|_K &= \det G_{h,p}(X)|_K . \end{aligned} \tag{12}$$

Therefore, in the isoparametric setting, the mapping to the physical domain is completely determined from the nodal positions of each element $\boldsymbol{x}_i^K$. To ensure the domain mapping is continuous, we only allow the nodal positions of the *continuous, high-order mesh*, denoted $\boldsymbol{x} \in \mathbb{R}^{N_{\boldsymbol{x}}}$, to vary. This ensures nodes co-located in the reference domain will be co-located in the physical domain. With this notation, the continuous domain mapping is parametrized by $\mu = \boldsymbol{x}$, i.e., $\Omega = \mathcal{G}(\Omega_0, \boldsymbol{x})$. The remainder of the document will use $\boldsymbol{x}$ to parametrize the domain deformation instead of μ. Finally, the integrals in (9) are evaluated using high-order Gaussian quadrature rules to yield the discrete form of the governing equations

$$\boldsymbol{r}(\boldsymbol{u}, \boldsymbol{x}) = 0, \tag{13}$$

where $\boldsymbol{u} \in \mathbb{R}^{N_{\boldsymbol{u}}}$ ($N_{\boldsymbol{u}} = N_p N_c |\mathcal{E}_{h,p}|$) is the solution vector comprised of the coefficients $\boldsymbol{u}_i^K$ for all elements.

III. High-order shock tracking via optimization-based r-adaptivity

In this section, we present an optimization framework designed to align discontinuous features in a finite-dimensional solution basis with features in the solution itself. In the discretization setting outlined in Section II, this amounts to aligning element faces, where discontinuities are supported, with discontinuities in the solution. With the discontinuous features tracked with element faces, very coarse high-order discretizations are effectively used to resolve the smooth solution throughout the domain. To align element faces with solution discontinuities, an optimization-based r-adaptivity framework is developed with an appropriate parametrization of the nodal positions of the continuous, high-order mesh, a shock tracking objective function, the discretized conservation law as the nonlinear equality constraints, and a full space PDE-constrained optimization solver to robustly solve the optimization problem. An overview of each of these components is provided in the remainder of this section; see [10] for a detailed description.

III.A. Optimization formulation for r-adaptivity

The goal of the r-adaptivity framework is to align faces of the DG mesh with the discontinuity. Since the discontinuity is not known *a-priori*, a mesh cannot be constructed to explicitly conform to the shock. Instead, we consider a parametrization of the nodal positions of the continuous, high-order mesh $\boldsymbol{x} = \boldsymbol{x}(\boldsymbol{\phi}) = \mathcal{A}(\boldsymbol{\phi})$, where $\boldsymbol{\phi} \in \mathbb{R}^{N_{\boldsymbol{\phi}}}$ is a vector of parameters. In the most general case, each degree of freedom of node of the mesh is an optimization parameter and $\mathcal{A}(\boldsymbol{\phi}) = \boldsymbol{\phi}$ is the identity map; however, the mapping $\mathcal{A}(\boldsymbol{\phi})$ can be

used to build any *a-priori* knowledge of the shock location into the parametrization or steps that ensure the resulting mesh is well-conditioned, e.g., smoothing.

With this parametrization, the problem of solving the discrete PDE on a fixed mesh, i.e., $\boldsymbol{r}(\boldsymbol{u};\, \boldsymbol{x}) = 0$ where $\boldsymbol{x}$ is given, is replaced with the optimization problem

$$\begin{aligned} \underset{\boldsymbol{u},\, \boldsymbol{\phi}}{\text{minimize}} \quad & f(\boldsymbol{u};\, \boldsymbol{x}(\boldsymbol{\phi})) \\ \text{subject to} \quad & \boldsymbol{r}(\boldsymbol{u};\, \boldsymbol{x}(\boldsymbol{\phi})) = 0, \end{aligned} \tag{14}$$

where $f(\boldsymbol{u};\, \boldsymbol{x})$ is a shock-indicating objective function. This optimization problem seeks to find the mesh $\boldsymbol{x}(\boldsymbol{\phi})$ and solution $\boldsymbol{u}$ that minimize $f(\boldsymbol{u},\, \boldsymbol{x})$ while satisfying the discretized PDE. The next section discusses our particular choice of the shock tracking objective function.

III.B. Shock tracking objective function

An effective objective function for the optimization formulation in (14) must monotonically approach a (local) minimum in the feasible set as $\boldsymbol{x} \to \boldsymbol{x}^*$, where $\boldsymbol{x}^*$ is any mesh that aligns with the shock. While residual-based error indicators are popular in the mesh adaptation community, we have observed that these fail to *monotonically* approach a local minima. The indicator used in this work is the integrated deviation of the solution from the mean in each element:

$$f_{shk}(\boldsymbol{u},\, \boldsymbol{x}) = h_0^{-2} \sum_{K \in \mathcal{E}_{h,p}} \int_{\mathcal{G}(K,\, \boldsymbol{x})} \left\| u_{h,p} - \bar{u}_{h,p}^K \right\|_{\boldsymbol{W}}^2 \, dV \tag{15}$$

where the dependence of the finite dimensional solution $u_{h,p}$ on the discrete representation is implied, $\bar{u}_{h,p}^K$ is the mean value of $u_{h,p}$ over element K, $\boldsymbol{W} \in \mathbb{R}^{N_c \times N_c}$ is the symmetric positive semi-definite matrix that defines the local semi-norm, and h_0 is the length scale of the mesh $\mathcal{E}_{h,p}$

$$\bar{u}_{h,p}^K = \frac{1}{|\mathcal{G}(K,\, \boldsymbol{x})|} \int_{\mathcal{G}(K,\, \boldsymbol{x})} u_{h,p} \, dV, \qquad |\mathcal{G}(K,\, \boldsymbol{x})| = \int_{\mathcal{G}(K,\, \boldsymbol{x})} dV, \qquad h_0 = \left(\frac{1}{|\mathcal{E}_{h,p}|} \int_{\Omega_0} dV \right)^{1/d}. \tag{16}$$

The h_0^{-2} factor ensures the indicator scales as $\mathcal{O}(1)$ instead of $\mathcal{O}(h^2)$. In this work, we only consider $\boldsymbol{W} = \boldsymbol{e}_1^T \boldsymbol{e}_1$ (density component). While this objective does not provably satisfy the required objective function conditions, it seems to satisfy them in practice; see [10] for additional detail.

The discontinuity indicator in (15) is not well-suited as the objective function in the discontinuity-tracking optimization setting (14) in its current form because it is agnostic to a poor quality or inverted mesh that may arise from certain choices of $\boldsymbol{x}$. Therefore we construct the objective function as a weighted combination of (15) and a function $f_{msh} : \mathbb{R}^{N_{\boldsymbol{x}}} \to \mathbb{R}$ that penalizes mesh distortion

$$f(\boldsymbol{u},\, \boldsymbol{x}) = f_{shk}(\boldsymbol{u},\, \boldsymbol{x}) + \alpha f_{msh}(\boldsymbol{x}). \tag{17}$$

In this work, we use the following mesh distortion measures

$$f_{msh}(\boldsymbol{x}) = \begin{cases} h_0 \displaystyle\sum_{K \in \mathcal{E}_{h,p}} \left| \frac{h_0}{|\mathcal{G}(K,\, \boldsymbol{x})|} - 1 \right| & d = 1 \\ h_0^d \displaystyle\sum_{K \in \mathcal{E}_{h,p}} \frac{1}{|\mathcal{G}(K,\, \boldsymbol{x})|} \int_{\mathcal{G}(K,\, \boldsymbol{x})} \left(\frac{\|G_{h,p}\|_F^2}{(\det G_{h,p})_+^{2/d}} \right)^r & \text{otherwise,} \end{cases} \tag{18}$$

where the h_0^d factor is included to ensure the f_{msh} scales independently of h and $r = 2$ is used in this work. The reader is referred to [10] for additional detail on the proposed objective function and a comparison with existing discontinuity indicators.

III.C. Full space optimization solver

Two standard approaches exist for solving PDE-constrained optimization problems such as the one in (14). The first, and most common, is known as the reduced space approach explicitly enforces the PDE constraint

at all times by defining $\boldsymbol{u}(\boldsymbol{x})$ as the solution of $\boldsymbol{r}(\boldsymbol{u}, \boldsymbol{x}) = 0$, which reduces (14) to an unconstrained optimization problem

$$\underset{\boldsymbol{\phi}}{\text{minimize}} \quad f(\boldsymbol{u}(\boldsymbol{x}(\boldsymbol{\phi})), \boldsymbol{x}(\boldsymbol{\phi})). \tag{19}$$

This approach cannot be used in this setting as $\boldsymbol{r}(\boldsymbol{u}, \boldsymbol{x}) = 0$ can only be solved if the mesh is perfectly aligned with the shock or enough viscosity is added to stabilize the solution. Since the mesh will not align with the shock until convergence of the optimization procedure, this approach can only be used if sufficient viscosity (or simply Laplacian-based diffusion) is added during intermediate iterations. The second approach, called the full space approach, treats the $\boldsymbol{u}$ and $\boldsymbol{\phi}$ as independent optimization variables, as suggested in (14), and converge them simultaneously to their optimal values. This implies the solution of the PDE is *never required away from a discontinuity-aligned mesh* $\boldsymbol{x}^*$ and overcomes the fundamental difficulty with the reduced space formulation. Therefore, the full space approach is the preferred method since the reduced space solver is extremely sensitivity to a heuristic, viscosity-based homotopy strategy. See [10] for further detail on the trade-off between the full and reduced space solvers.

IV. Applications

IV.A. Transonic, inviscid flow through nozzle

The proposed high-order shock tracking framework is applied to the nonlinear, quasi-one-dimensional Euler equations that model inviscid, compressible flow in a variable-area stream tube $A(x)$

$$\frac{\partial}{\partial x}(\rho u) = -\frac{1}{A}\frac{\mathrm{d}A}{\mathrm{d}x}\rho u, \tag{20}$$

$$\frac{\partial}{\partial x}(\rho u^2 + p) = -\frac{1}{A}\frac{\mathrm{d}A}{\mathrm{d}x}\rho u^2, \tag{21}$$

$$\frac{\partial}{\partial x}([\rho E + p]u) = -\frac{1}{A}\frac{\mathrm{d}A}{\mathrm{d}x}(\rho E + p)u \tag{22}$$

where ρ is the fluid density, u is the fluid velocity, p is the thermodynamic pressure, and

$$\rho E = \rho e + \frac{1}{2}\rho u^2 \tag{23}$$

is the total energy. The pressure is related to ρE by the equation of state

$$p = (\gamma - 1)\left(\rho E - \frac{1}{2}\rho u^2\right) \tag{24}$$

for a perfect gas with ration of specific heats $\gamma = 1.4$. The domain is taken as $\Omega = (0, 1)$ and the nozzle profile takes the form

$$A(x) = \begin{cases} 1 - (1 - T)\cos(\pi(x - 0.5)/0.8)^2 & x \in [0.1, 0.9] \\ 1 & \text{otherwise} \end{cases} \tag{25}$$

where $T = 0.6$ is the height of the nozzle throat. The boundary conditions weakly impose the farfield conditions $\rho_i = 1.0$, $u_i = 1.0$, $M_i = 0.40$ at the inflow and $\rho_o = 1.0$, $u_o = 1.0$, $M_o = 0.42$ at the outflow using the approximate Riemann solver. The reference solution, given in Figure 2, was computed on a highly adapted mesh near the discontinuity consisting of over 8000 linear ($p = 1$) elements. The test case was chosen such that the shock is sufficiently weak that the oscillations did not cause the nonlinear iterations to diverge or encounter negative density or pressure values.

The proposed discontinuity-tracking framework is applied to solve the quasi-1d Euler equations using very few high-order elements. The full space optimization approach discussed in Section III.C is used and SNOPT [14] is used as the nonlinear optimizer. The results are shown in Figure 3, where only 4 quadratic ($p = 2$), cubic ($p = 3$), and quartic ($p = 4$) elements are used. While the $p = 2$ and $p = 3$ cases are somewhat underresolved, the $p = 4$ case matches the reference solution very closely.

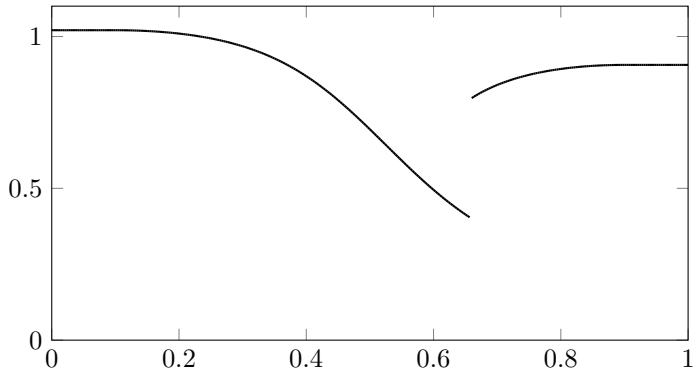

Figure 2: Reference solution with 300 $p = 1$ elements.

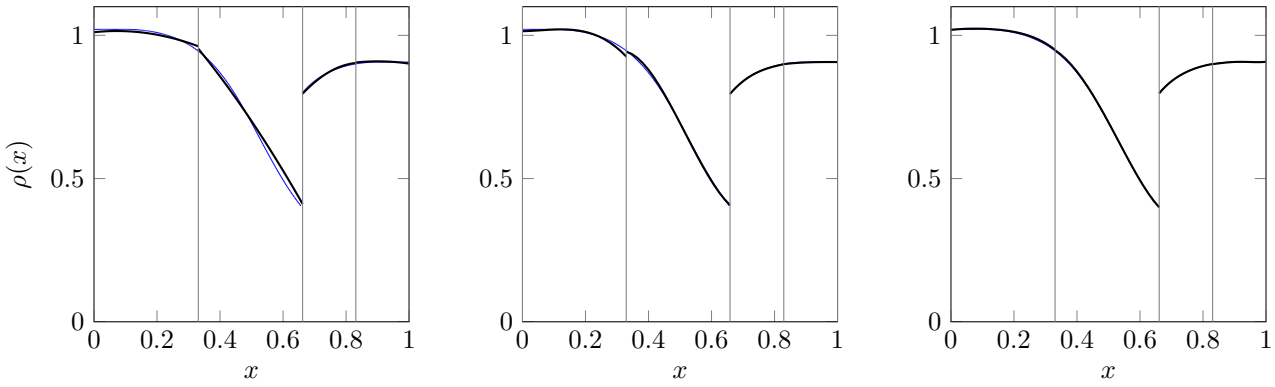

Figure 3: The solution of the quasi-1d Euler equations using the proposed high-order DG shock tracking framework using the full space optimization approach with SNOPT as the chosen optimizer. Only 4 quadratic (left), cubic (middle), and quartic (right) are used. The vertical lines (——) indicate the element boundaries with the corresponding solution in black (——) and the reference solution using over 8000 linear elements in blue (——).

IV.B. Supersonic flow around two-dimensional bluff body

In this section, we study the performance of the proposed discontinuity tracking framework on two-dimensional inviscid, supersonic flow around a rounded square. The geometry of the domain and reference mesh with $|\mathcal{E}_{h,p}| = 102$ elements are shown in Figures 4 for polynomial orders $p = 1$, $p = 2$, and $p = 3$. The flow is

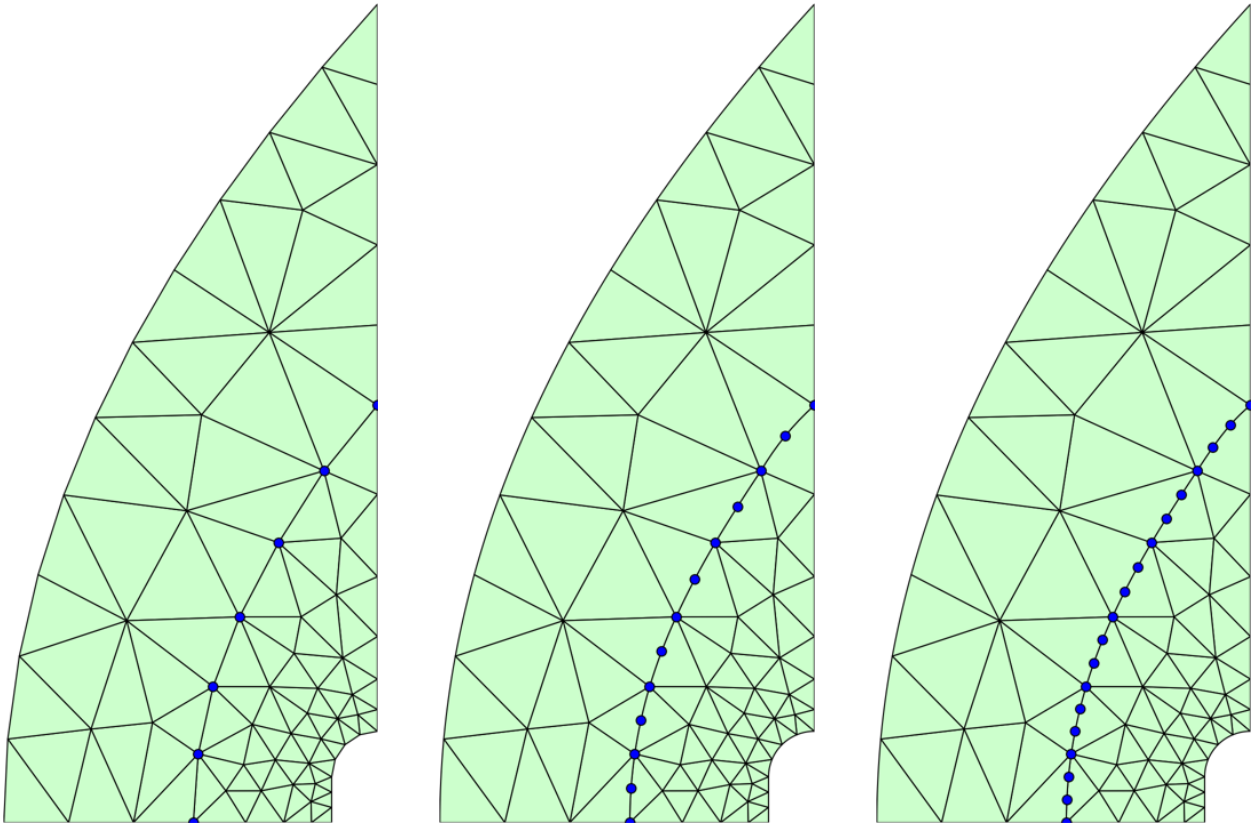

Figure 4: Reference domain and mesh with $|\mathcal{E}_{h,p}| = 102$ elements and polynomial orders $p = 1$ (*left*), $p = 2$ (*center*), $p = 3$ (*right*). The blue circles identify parametrized nodes, i.e., nodal positions that whose displacements compose the optimization variables $\boldsymbol{\phi}$. Only the displacement normal to the boundary are taken as optimization variables for the two parametrized nodes that lie on boundaries.

modeled by the two-dimensional steady Euler equations

$$\begin{aligned} \frac{\partial}{\partial x_i}(\rho u_i) &= 0, \\ \frac{\partial}{\partial x_i}(\rho u_i u_j + p) &= 0 \quad \text{for } i = 1, 2, \\ \frac{\partial}{\partial x_i}\left(u_j(\rho E + p)\right) &= 0, \end{aligned} \tag{26}$$

where ρ is the fluid density, u_1, u_2 are the velocity components, and E is the total energy. For an ideal gas, the pressure p has the form

$$p = (\gamma - 1)\rho\left(E - \frac{1}{2}u_k u_k\right), \tag{27}$$

where γ is the adiabatic gas constant. The discretization of the governing equations proceed according to the formulation in Section II and Roe's approximate Riemann solver corresponding to the time-dependent version of (26) is used for the numerical flux. All farfield and inviscid wall boundary conditions are weakly imposed using the Roe solver. The incoming flow is taken as supersonic at Mach 4.

For simplicity, we use a simple mesh parametrization that does not include the position of all the nodes of the continuous high-order mesh, but rather a well-chosen subset of these nodes. The remainder of the

nodes are determined through a linear operator that incorporates mesh smoothing. In this work, we use linear elasticity with prescribed displacements at the parametrized nodes and in the normal direction along domain boundaries. The free degrees of are shown in Figure 4 and lead to $N_{\boldsymbol{\phi}} = 12$ for $p = 1$, $N_{\boldsymbol{\phi}} = 24$ for $p = 2$, and $N_{\boldsymbol{\phi}} = 36$ for $p = 3$.

As a non-convex optimization problem underlies the discontinuity-tracking framework, the performance of the full space solver relies on a quality initial guess. In [10], we used the reference mesh as the initial guess for $\boldsymbol{\phi}$ and the solution of the conservation law on this non-aligned mesh, with sufficient viscosity added such that it can be computed, as the initial guess for $\boldsymbol{u}$ for the $p = 1$ case. However, in the present case the shock is quite strong given the large Mach number ($M = 4$) and the viscosity required to stabilize the solution on this mesh provides a meaningless initial guess. Therefore, we use homotopy in the Mach number to provide a reasonable starting guess for the $M = 4$ problem at polynomial order $p = 1$. That is, we solve the discontinuity-tracking problem at $M = 3$ and use the ($\boldsymbol{u}$, $\boldsymbol{\phi}$) solution as the initial guess for the $M = 4$ case. Similarly, the $M = 3$ problem is initialized from the solution of the $M = 2.5$ problem. The shock in the $M = 2.5$ case is sufficiently weak that the viscosity solution provides a reasonable starting guess. Similar to [10], we use homotopy in p to initialize the discontinuity-tracking problems for polynomial orders beyond 1. That is, the discontinuity-tracking solution at polynomial order p is used to initialize the solver at polynomial order $p + 1$. This requires a simple injection operation to transfer the solution $\boldsymbol{u}$ and mesh $\boldsymbol{x}(\boldsymbol{\phi})$ to a higher polynomial degree.

The result of the discontinuity-tracking method using the above initialization strategy and the reference domain in Figure 4 is provided in Figure 5. For all polynomial orders, the shock is tracked as well as possible given the resolution limit of the mesh and all elements are high-quality. The solution for the $p = 1$ mesh is clearly underresolved and the shock surface is faceted since the elements cannot bend in the piecewise linear setting. The $p = 2$ and $p = 3$ meshes deliver quite accurate and smooth solutions solutions away from the shock and track the smooth, curved shock surface very well.

The total enthalpy, $H = (\rho E + p)/\rho$, is constant in steady inviscid flow and therefore we use the following error metric to quantify the performance of the discontinuity tracking framework without requiring a reference solution

$$e_H = \sqrt{\frac{\int_\Omega (H - H_0)^2 \, dv}{\int_\Omega dv}}, \tag{28}$$

where H_0 is the farfield enthalpy. Table 1 shows the discontinuity-tracking framework provides accurate solutions on discretizations with very few degrees of freedom, e.g., $N_{\boldsymbol{u}} \sim \mathcal{O}(10^3)$ with errors on the order of $e_H \sim \mathcal{O}(10^{-3})$.

Polynomial order (p)	Number of degrees of freedom ($N_{\boldsymbol{u}}$)	Enthalpy error (e_H)
1	1224	1.517×10^{-3}
2	2448	5.745×10^{-4}
3	4080	4.408×10^{-4}

Table 1: Discontinuity-tracking performance summary, including the number of degrees of freedom and the enthalpy error for the reference mesh in Figure 4 with 102 elements and polynomials orders $p = 1$, $p = 2$, $p = 3$.

V. Conclusion

This document presented a high-order accurate, nonlinearly stable discontinuity-tracking framework for solving conservation laws with discontinuous solution features. The method leverages the discontinuities between elements present in the finite-dimensional solution basis in the context of a discontinuous Galerkin discretization to track discontinuities in the underlying solution. The approximate Riemann solvers ensure the numerical fluxes are consistent with the governing equations and provide appropriate stabilization through upwinding. Central to the tracking framework is a PDE-constrained optimization formulation of the discrete conservation law whose objective pushes the mesh to align with discontinuities and constraints ensure the discrete conservation law is satisfied. The proposed objective function not only attains its minimum when the mesh is aligned with discontinuities, but also approaches the minimum monotonically, which is critical for a gradient-based optimizer to locate it. The optimization problem is solved using a full space

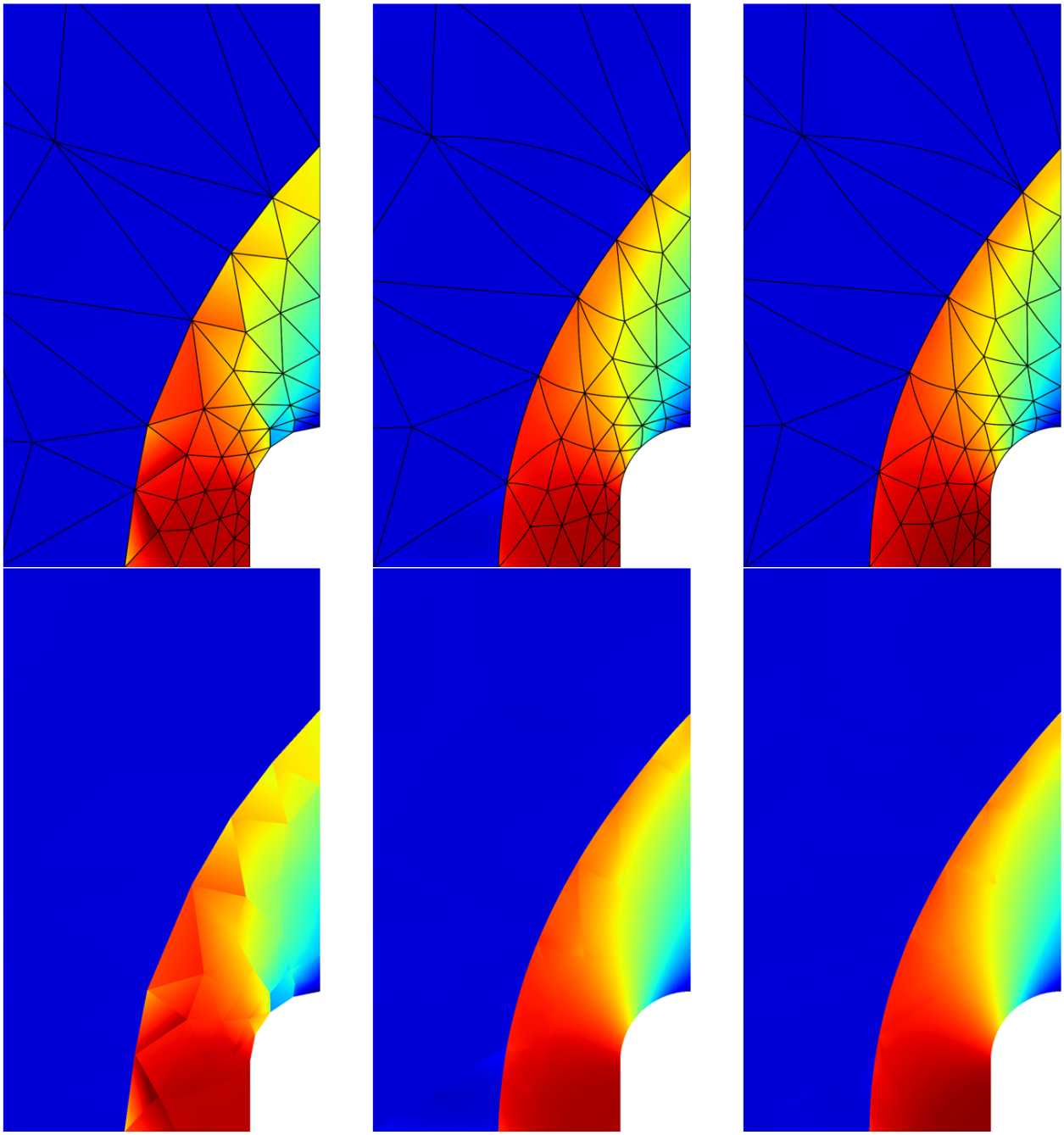

Figure 5: Solution of two-dimensional Euler equations (density) with supersonic inflow $M = 4$ using discontinuity-tracking framework with polynomial orders $p = 1$ (*left*), $p = 2$ (*center*), $p = 3$ (*right*). The deformed mesh provided by the tracking framework is included in the *top row* to show the high-quality curved elements that track the shock location. The mesh is not included in the *bottom row* to clearly show the solution features away from the shock.

optimization solver whereby the PDE solution and mesh simultaneously converge to their optimal values, ensuring the discrete PDE solution is never required on non-aligned meshes. The merit of the method is established on a one and two dimensional test problem where accurate solutions were obtained on coarse meshes. For the two dimensional problem, the mesh *curved* to define the shock surface and a highly accurate solution to a supersonic, Mach 4 problem was obtained with only 102 cubic elements.

A number of important research directions must be investigated if the proposed framework is to be a viable approach for resolving problems with discontinuous solutions. First, there is considerable structure in the optimization problem (14), e.g., only equality constraints, partition of optimization variables in $\boldsymbol{u}$ and $\boldsymbol{\phi}$, invertible constraint Jacobian with respect to $\boldsymbol{u}$, efficient sparse parallel solvers available for operations involving $\boldsymbol{r}$ and its derivatives, that black-box optimizers cannot leverage. Therefore we intend to develop a solver that can leverage this structure and incorporate well-known homotopy strategies into the constraint since $\boldsymbol{r}(\boldsymbol{u}, \boldsymbol{x}) = 0$ is difficult to solve for high-speed flows that contain discontinuities. There is also potential to speed up the proposed solver and improve the quality of the resulting mesh by incorporating local topology changes at discrete times during the optimization solve. Additionally, testing on complex flows in two- and three-dimensions is required.

Acknowledgments

This work was supported in part by the Luis W. Alvarez Postdoctoral Fellowship (MZ) by the Director, Office of Science, Office of Advanced Scientific Computing Research, U.S. Department of Energy under Contract No. DE-AC02-05CH11231 (MZ, PP) and by the AFOSR Computational Mathematics program under grant number FA9550-15-1-0010 (MZ, PP). The content of this publication does not necessarily reflect the position or policy of any of these supporters, and no official endorsement should be inferred.

References

[1]Cockburn, B. and Shu, C.-W., "Runge-Kutta discontinuous Galerkin methods for convection-dominated problems," *J. Sci. Comput.*, Vol. 16, No. 3, 2001, pp. 173–261.

[2]Hesthaven, J. S. and Warburton, T., *Nodal discontinuous Galerkin methods*, Vol. 54 of *Texts in Applied Mathematics*, Springer, New York, 2008, Algorithms, analysis, and applications.

[3]Peraire, J. and Persson, P.-O., *Adaptive High-Order Methods in Computational Fluid Dynamics*, Vol. 2 of *Advances in CFD*, chap. 5 – High-Order Discontinuous Galerkin Methods for CFD, World Scientific Publishing Co., 2011.

[4]Baumann, C. E. and Oden, J. T., "A discontinuous *hp* finite element method for the Euler and Navier-Stokes equations," *Int. J. Numer. Methods Fluids*, Vol. 31, No. 1, 1999, pp. 79–95, Tenth International Conference on Finite Elements in Fluids (Tucson, AZ, 1998).

[5]Burbeau, A., Sagaut, P., and Bruneau, C.-H., "A problem-independent limiter for high-order Runge-Kutta discontinuous Galerkin methods," *J. Comput. Phys.*, Vol. 169, No. 1, 2001, pp. 111–150.

[6]Shu, C.-W. and Osher, S., "Efficient implementation of essentially nonoscillatory shock-capturing schemes," *J. Comput. Phys.*, Vol. 77, No. 2, 1988, pp. 439–471.

[7]Persson, P.-O. and Peraire, J., "Sub-Cell Shock Capturing for Discontinuous Galerkin Methods," *44th AIAA Aerospace Sciences Meeting and Exhibit, Reno, Nevada*, 2006, AIAA-2006-0112.

[8]Persson, P.-O., "Shock Capturing for High-Order Discontinuous Galerkin Simulation of Transient Flow Problems," *21st AIAA Computational Fluid Dynamics Conference, San Diego, CA*, Jun 2013, AIAA-2013-3061.

[9]Von Neumann, J. and Richtmyer, R. D., "A method for the numerical calculation of hydrodynamic shocks," *J. Appl. Phys.*, Vol. 21, 1950, pp. 232–237.

[10]Zahr, M. J. and Persson, P.-O., "An optimization-based approach for high-order accurate discretization of conservation laws with discontinuous solutions," *submitted*, 2017.

[11]Persson, P.-O., Bonet, J., and Peraire, J., "Discontinuous Galerkin solution of the Navier–Stokes equations on deformable domains," *Computer Methods in Applied Mechanics and Engineering*, Vol. 198, No. 17, 2009, pp. 1585–1595.

[12]Roe, P. L., "Approximate Riemann solvers, parameter vectors, and difference schemes," *Journal of computational physics*, Vol. 43, No. 2, 1981, pp. 357–372.

[13]Harten, A. and Hyman, J. M., "Self adjusting grid methods for one-dimensional hyperbolic conservation laws," *Journal of computational Physics*, Vol. 50, No. 2, 1983, pp. 235–269.

[14]Gill, P. E., Murray, W., and Saunders, M. A., "SNOPT: An SQP algorithm for large-scale constrained optimization," *SIAM Journal on Optimization*, Vol. 12, No. 4, 2002, pp. 979–1006.